Connecting the Atlantic Meridional Overturning Circulation to the Southern Ocean Following the Closure of Equatorial Seaways During the Cenozoic

Erwan Pineau[1] [ID], **Camille Lique[2]** [ID], **David Ferreira[3]** [ID], **Thierry Huck[2]** [ID], **Jean-Baptiste Ladant[4,5]** [ID], **Emma Fabre[4,5]**, **Jeanne Millot-Weil[6]**, and **Yannick Donnadieu[1]** [ID]

[1]Centre Européen de Recherche et d'Enseignement en Géosciences de l'Environnement, Aix-en-Provence, France, [2]Laboratoire d'Océanographie Physique et Spatiale (LOPS, UMR 6523), University Brest, CNRS, Ifremer, IRD, IUEM, Plouzané, France, [3]Department of Meteorology, University of Reading, Reading, UK, [4]Laboratoire des Sciences du Climat et de l'Environnement, CEA-CNRS-UVSQ, UMR 8212, Université Paris-Saclay, Gif-sur-Yvette, France, [5]Institut Pierre-Simon Laplace, Université Versailles Saint-Quentin, Guyancourt, France, [6]School of Geographical Sciences, University of Bristol, Bristol, UK

Abstract Global ocean circulation regulates climate and has undergone significant changes over the Cenozoic. Today, the Atlantic Meridional Overturning Circulation (AMOC) is driven by North Atlantic Deep Water (NADW) formation and Southern Ocean upwelling. By contrast, during the middle Eocene to early Oligocene (48–28 Ma), a restricted Drake Passage was limiting the northern Ekman transport, while a circum-equatorial current sustained by trade winds promoted low-latitude upwelling. Our set of simulations with the IPSL-CM5A2 model reveals that this paleogeographic setting favored proto-NADW upwelling at low latitudes, confining the AMOC to the Northern Hemisphere. Consequently, the role of southern westerly winds was limited, and the northward heat transport was weaker than in the modern ocean.

Plain Language Summary Ocean currents redistribute heat globally and are central to regulating Earth's climate. Today, the Atlantic Meridional Overturning Circulation (AMOC) is a key system, carrying warm, salty surface waters northward and returning cold deep waters southward, which ultimately upwell near Antarctica under the influence of Southern Ocean winds and currents. However, this circulation has evolved over geological times. Between 48 and 28 million years ago, from the Eocene to the Oligocene, continental configurations and ocean gateways differed markedly. Narrow Antarctic passages and open tropical seaways reshaped global circulation. Our study shows that during this period, deep water upwelled near the Equator, restricting the AMOC to the North Atlantic. Consequently, winds and ocean currents in the Southern Ocean exerted far less influence on the AMOC than they do today.

1. Introduction

Solar radiation unevenly heats the Earth's surface, creating a latitudinal imbalance in the global energy budget. To counteract this imbalance, atmospheric and oceanic circulations redistribute heat from the equator to the poles (Meyssignac et al., 2019). In today's climate, the Atlantic Ocean hosts the most active upper branch of the Meridional Overturning Circulation (MOC; Johnson et al., 2019). Warm tropical surface waters flow northward, gradually losing buoyancy through air-sea interactions, and eventually reach regions of weak vertical stratification (Johnson et al., 2019; Klocker et al., 2023). This leads to seasonal deepening of the mixed layer, extending to depths of approximately 1–3 km in winter, and the formation of dense water masses such as the North Atlantic Deep Water (NADW; Johnson et al., 2019). NADW is advected southward until it resurfaces in the Southern Hemisphere via wind-driven upwelling (J. Marshall & Speer, 2012). The lower cell of the MOC is sustained by dense water formation in the Southern Ocean and is referred to as the Southern Ocean MOC (SOMOC; Talley, 2013).

In the present climate, the Southern Ocean plays a central role in regulating the Atlantic MOC (AMOC), being the only region where the Atlantic, Pacific, and Indian oceans are connected by the Antarctic Circumpolar Current (ACC; see the review by J. Marshall & Speer, 2012). Westerly winds over the Southern Ocean drive a northward Ekman transport at the surface, balanced by a deep geostrophic return flow, generating a surface divergence compensated by upwelling of mid-depth waters (Johnson et al., 2019). Gnanadesikan (1999) developed a

Software: Jean-Baptiste Ladant, Emma Fabre, Jeanne Millot-Weil
Supervision: Camille Lique, Yannick Donnadieu
Validation: Erwan Pineau, Camille Lique, David Ferreira, Thierry Huck, Jean-Baptiste Ladant, Yannick Donnadieu
Visualization: Erwan Pineau
Writing – original draft: Erwan Pineau
Writing – review & editing: Erwan Pineau, Camille Lique, David Ferreira, Thierry Huck, Jean-Baptiste Ladant, Emma Fabre, Yannick Donnadieu

theoretical framework emphasizing the role of Southern Ocean winds and mesoscale eddies in shaping the pycnocline structure throughout the Atlantic and modulating NADW formation. Cessi (2019) highlighted that the formation of NADW is tied to the strength of Ekman transport in the Southern Ocean, which in turn is controlled by wind intensity. Similarly, Shakespeare and Hogg (2012) introduced a three-layer analytical model in which the AMOC intensity scales linearly with the Southern Ocean wind stress, and the ACC transport is approximated by the sum of Ekman and abyssal overturning components. Using a simple thermal wind balance linking AMOC and ACC strengths to three key depths (the pycnocline, the AMOC maximum, and the wind-driven ACC), D. P. Marshall and Johnson (2017) predicted an ACC/AMOC ratio of 8 ± 4 for present-day conditions. This matches observational estimates, indicating that these depths capture the main dynamics governing their coupling. The AMOC strength and structure further control the magnitude of the meridional heat transport (MHT), with an estimated ratio of 0.05–0.08 PW/Sv (Wang et al., 2023).

At the beginning of the Cenozoic (66 million years ago, Ma), the Atlantic Ocean was relatively narrow, but gradually widened over time (Labails et al., 2010). Additionally, equatorial oceanic gateways were wide and deeper than 1,000 m in the early Cenozoic, but progressively narrowed or closed throughout the era (Jaramillo, 2018). In contrast, the gateways linking the Arctic and the North Atlantic—the Fram Strait and the Greenland-Scotland Ridge—began to gradually open in the late Eocene (Straume et al., 2020), while the Southern Ocean gateways were initially closed but started to open and deepen during the Eocene (Straume et al., 2020). These tectonic reorganizations reshaped inter-basin connectivity and had major consequences for global ocean circulation. Neodymium (Nd) records from the Pacific Ocean suggest that, between ∼70 and 30 Ma, deep water formation took place in the southern and northern Pacific (Thomas et al., 2014). The earliest evidence interpreted as the onset of deep circulation in the North Atlantic dates back to the early to middle Eocene (49–47 Ma) (Boyle et al., 2017; Hohbein et al., 2012). However, a number of recent studies point to the onset of deep water formation during the Eocene-Oligocene Transition (EOT; 34 Ma) (Borrelli et al., 2014; Coxall et al., 2018), coinciding with a rapid global cooling, the opening of the Drake Passage and Tasman Gateway, and the onset of the Antarctic Ice Sheet (AIS; Hutchinson et al., 2021). Once established, the proto-AMOC gradually evolved toward a modern-like configuration in terms of structure and intensity, particularly after ∼9 Ma during the late Miocene, in response to the closure of major equatorial oceanic gateways such as the Central American Seaway (CAS; Kirillova et al., 2019; Jaramillo, 2018). The reader is referred to Ferreira et al. (2018) for a detailed review of the AMOC evolution across the Cenozoic (their Figure 3).

As part of the Deep-Time Model Intercomparison Project, six out of eight models simulate a SOMOC under early Eocene paleogeographic conditions. Among these six, MIROC simulates a proto-AMOC, while CESM simulates a PMOC (Zhang et al., 2022). In contrast, the NorESM model simulates only a proto-AMOC, and the GFDL model produces only a PMOC (Zhang et al., 2022). All simulated proto-AMOC and PMOC circulations remain confined to the Northern Hemisphere. Meanwhile, six out of 14 MioMIP (Miocene MIP) simulations have an inter-hemispherical AMOC, and three simulations exhibit an inter-hemispherical PMOC during the early and middle Miocene (Naik et al., 2025). Assuming the AMOC was active, it expanded into the Southern Hemisphere between the early Eocene and the Miocene, aligning with the closure of low-latitude ocean passages (Zhang et al., 2022; Hotinski & Toggweiler, 2003; von der Heydt & Dijkstra, 2008). Yet, because of the diversity of the MIPs models, it remains difficult to determine the role of bathymetric constraints for the triggering and driving mechanisms of the AMOC in the different geological era.

In the following, we analyze the behavior of AMOC across five representative time slices: the middle Eocene (∼40 Ma), the early Oligocene (∼30 Ma), the early Miocene (∼20 Ma), the late Miocene (∼10 Ma), and the pre-industrial (PI) period. Using a unique suite of simulations from a single state-of-the-art coupled climate model with coherent paleogeographic reconstructions, we examine Cenozoic ocean dynamics changes and focus on the experiments that simulate an AMOC to study its structural evolution. The primary objective of our study is to assess whether the dynamical relationship between the ACC and the AMOC transports remain constant under varying paleoclimatic and paleogeographic conditions, which is crucial for understanding the long-term stability of large-scale ocean circulation dynamics. We will also evaluate the efficiency of the AMOC in transporting heat northward throughout the Cenozoic, which has major implications for Earth's climate evolution.

Table 1
Simulation Parameters: pCO_2, Antarctic and Greenland Ice-Sheets (AIS and GIS) Configurations

Period simulation	PI	10 Ma			20 Ma			
		10 Ma	10 Ma_BerO	10 Ma_CASO	20 Ma	20 Ma_ND	30 Ma	40 Ma
pCO_2 [ppmv]	280		420			560	560	840
AIS	Yes		Yes			Yes	Yes	No
GIS	Yes		Yes			No	No	No
GMST [°C]	14.2	17.2	17.2	17.1	19.6	19.5	19.9	23.9
T_{AMOC} [Sv]	11	15	13	14	8	7	18	18
T_{ACC} [Sv]	122	117	118	131	91	71	61	(53)
T_{CEC} [Sv]	–	–	–	–	4	2	16	56
T_{ACC}/T_{AMOC}	11	8	9	9	11	10	3	(3)

Note. Simulations results: the Global Mean Surface Temperature (GMST), the intensity of the maximum AMOC (T_{AMOC}) deeper than 200 m in the Northern Hemisphere, eastward volume transport of the ACC (T_{ACC}) between South Africa and Antarctica, and westward volume transport of the Circum-Equatorial Current (T_{CEC}) through the CAS, and the ratio between T_{ACC} and T_{AMOC}. T_{ACC} and T_{ACC}/T_{AMOC} at 40 Ma are between parenthesis because T_{ACC} at this period, reflects the eastern flow of the South Atlantic subpolar gyre intensity. Sensitivity experiments: Open Bering Strait (10 Ma_BerO), Open Central American Seaway (10 Ma_CASO) and Narrow Drake Passage (20 Ma_ND).

2. Methods

2.1. Model Description

The Earth System Model used in this study is the IPSL-CM5A2 model (Sepulchre et al., 2020), developed by the Institut Pierre-Simon Laplace for the fifth phase of the Coupled Model Intercomparison Project 5. The model couples several components: the atmospheric model LMDZ (Hourdin et al., 2013), the land surface and vegetation model ORCHIDEE (Krinner et al., 2005) and the ocean model NEMO (Madec et al., 2016). NEMO includes the general circulation model OPA8.2 and the sea ice model LIM2 (Fichefet & Maqueda, 1997). The resolution of the atmospheric grid is 3.75° in longitude and 1.875° in latitude, with 39 vertical layers. The ocean component uses 31 vertical layers, ranging from 10 m near the surface to 500 m at depth. The horizontal resolution is 2° in longitude and ranges in latitude from 0.5° near the Equator to 2° at high latitudes. Additional details about the ocean grid and the ocean-atmosphere coupler are given in Text S1 in Supporting Information S1.

2.2. Simulations

Paleogeographic boundary conditions follow the consistent set from Poblete et al. (2021) and Aminov et al. (2023). The bathymetry, the atmospheric CO_2 concentrations (pCO_2) and ice-sheet configurations for each simulation are detailed in Table 1 and Figures S1, S2, and S3 in Supporting Information S1. In addition to the baseline simulations, three sensitivity experiments were performed: two at 10 Ma, one with an open Bering Strait ("10 Ma_BerO"), one with an open CAS ("10 Ma_CASO") and a third one at 20 Ma with a Narrowed Drake Passage ("20 Ma_ND"). These share all parameters with the simulations from their respective baseline period (Table 1). The rationale for performing these sensitivity experiments is discussed in Text S1 in Supporting Information S1. The simulation details as well as the bathymetric differences are shown in Figure S4 in Supporting Information S1.

All simulations were run for at least 2,500 years to ensure climate quasi-equilibrium, particularly for the deep ocean temperatures (Figure S5 in Supporting Information S1; de Boer et al., 2025). Our analyses are based on the climatological means of the final 100 years of each simulation.

3. Results

We start by examining the mean Meridional Overturning Stream-Function (ψ) from the five simulations (Figure 1). $\psi(y, z)$ is calculated as:
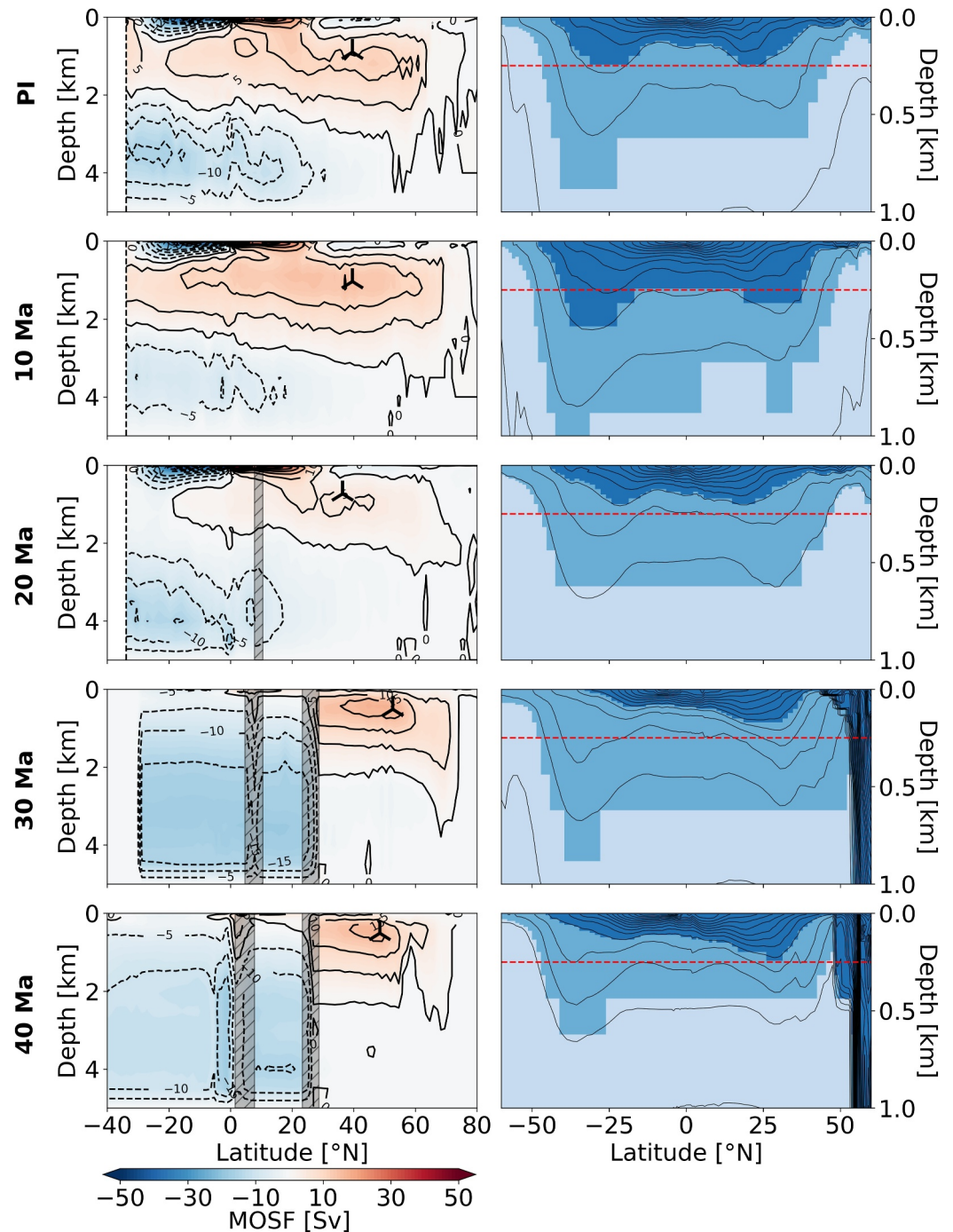
Figure 1. Left column: Meridional overturning stream-function in the Atlantic Ocean. Crosses indicate the location of the maximum intensity of the Atlantic Meridional Overturning Circulation. The latitude of the southern tip of Africa is represented by the southernmost dashed line and the latitudes of the CAS and Gibraltar are represented by the hatched zones. Right column: Zonally and annually-averaged isopycnals in the Atlantic Ocean. The dark and sky blue shadings highlight isopycnals outcropping in the North and South Atlantic respectively, the light blue corresponds to non-outcropping isopycnals. These water masses were found by identifying the maximal ocean density at the surface in the North and South Atlantic separately and considering water masses lighter than this maximal value. The horizontal dashed red lines at 250 m correspond to the depth reached in the South subtropical latitudes by the isopycnals outcropping in the North Atlantic for the PI period.

$$\psi(y,z) = \int_{\lambda_w}^{\lambda_e} \int_z^0 v(x,y,z')\,dz'\,dx \tag{1}$$

with v the meridional velocities, λ_w and λ_e the western and eastern Atlantic boundaries, respectively. Because ψ in Equation 1 is only meaningful when the transport is non-divergent in the (y,z) plane, we mask out regions where the Atlantic is open zonally (see Figure 1).

Across all five periods, the simulations show an AMOC along with a SOMOC cell (Figure 1). The AMOC exhibits a clear inter-hemispheric structure in the PI, 10 Ma, and 20 Ma simulations, with deep water formation sites, of which the Mixed Layer Depth is a proxy, located in the Nordic Seas (Figure S6 in Supporting Information S1).

In contrast, the AMOC is confined to the Northern Hemisphere in the 30 Ma and 40 Ma simulations, with low-latitude upwelling of NADW between 23°N and 29°N, corresponding to the latitudes of the Gibraltar Strait (Figure 1). At 30 and 40 Ma, the northern deep water formation sites are mainly located in the Labrador Sea (Figure S6 in Supporting Information S1) and the restriction of the AMOC to the Northern Hemisphere appears to favor the expansion of the SOMOC cell (Figure S7 in Supporting Information S1). At 20 Ma, the SOMOC is active along with the inter-hemispheric AMOC. This is potentially due to the configuration of the low-latitude straits, with a closed Eastern Tethys Seaway and an open CAS. The maximum AMOC intensities are 11 Sv for PI, 15 Sv for 10 Ma, 8 Sv for 20 Ma, and 18 Sv in both the 30 Ma and 40 Ma simulations (Table 1). The two sensitivity experiments at 10 Ma ("10 Ma_BerO" and "10 Ma_CASO") simulate a slightly weaker AMOC relative to the 10 Ma simulation (14 and 13 Sv respectively; Table 1 and Figure S8 in Supporting Information S1). At 20 Ma, the experiment "20 Ma_ND" simulates a weaker AMOC relative to the 20 Ma simulation (7 Sv; Table 1 and Figure S8 in Supporting Information S1).

The existence of an AMOC is not a consistent feature among models, as discussed in the Introduction (Naik et al., 2025; Zhang et al., 2022), and it is highly sensitive to the connectivity between the Arctic and Atlantic oceans (Hutchinson et al., 2018; Straume et al., 2022; Vahlenkamp et al., 2018). In this study, we employed a consistent set of paleogeographic reconstructions (Aminov et al., 2023; Poblete et al., 2021) featuring a closed Greenland–Scotland Ridge at 30 and 40 Ma (Straume et al., 2020), which prevents Arctic freshwater outflow into the North Atlantic deep-water formation regions (Figure S9 in Supporting Information S1). As a result, the enclosed or semi-enclosed Arctic Ocean exhibits a very low sea surface salinity at 30 and 40 Ma, as it accumulates the substantial net surface freshwater input from net precipitation and runoff (Figure S9 in Supporting Information S1, more details in Text S1 in Supporting Information S1).

Along with changes of the AMOC, the stratification of the water column has also strongly evolved across the Cenozoic, with large changes affecting both the depth of the pycnocline and the isopycnal slopes in the Atlantic (Figure 1). In the PI experiment, isopycnals corresponding to the main pycnocline (i.e., the boundary between light, low-latitude originating surface waters and dense, high-latitude abyssal waters) are close to the surface around Antarctica and tilt across the ACC under the influence of the southern westerly winds, reaching 250 m. Note that recent work indicates that buoyancy loss and deep water formation in the North Atlantic also modulate the pycnocline depth (Nayak et al., 2024). Regardless of the driving mechanism, isopycnals remain relatively flat across most latitudes until they shoal at high latitudes (Figure 1), consistent with the theoretical predictions by Gnanadesikan (1999); Nikurashin and Vallis (2012).

Our PI and 10 Ma experiments exhibit similar Atlantic isopycnal structures, with steep slopes marking the region of maximum ACC transport between 30°S and 50°S (Figure 1). In these two simulations, isopycnals outcropping in the North Atlantic reach depths of approximately 250 m between 20°S and 35°S, while these isopycnals are restricted to depths shallower than 200 m at 30 and 40 Ma (Figure 1). In contrast, outcropping depths of the isopycnals outcropping in the North Atlantic range from 200 to 300 m across all experiments between 20°N and 35°N.

The Barotropic Stream-function (BSF) describes the vertically integrated ocean circulation and shows the intrinsic connection between vertical (overturning) and horizontal (gyre) circulations (Figure 2). The PI, 10 Ma, and 20 Ma experiments display well-developed subtropical and subpolar gyres in the North Atlantic, whereas at 30 Ma and 40 Ma, the gyres are weaker, smaller and accompanied by an equatorial through-flow (Figure 2). These
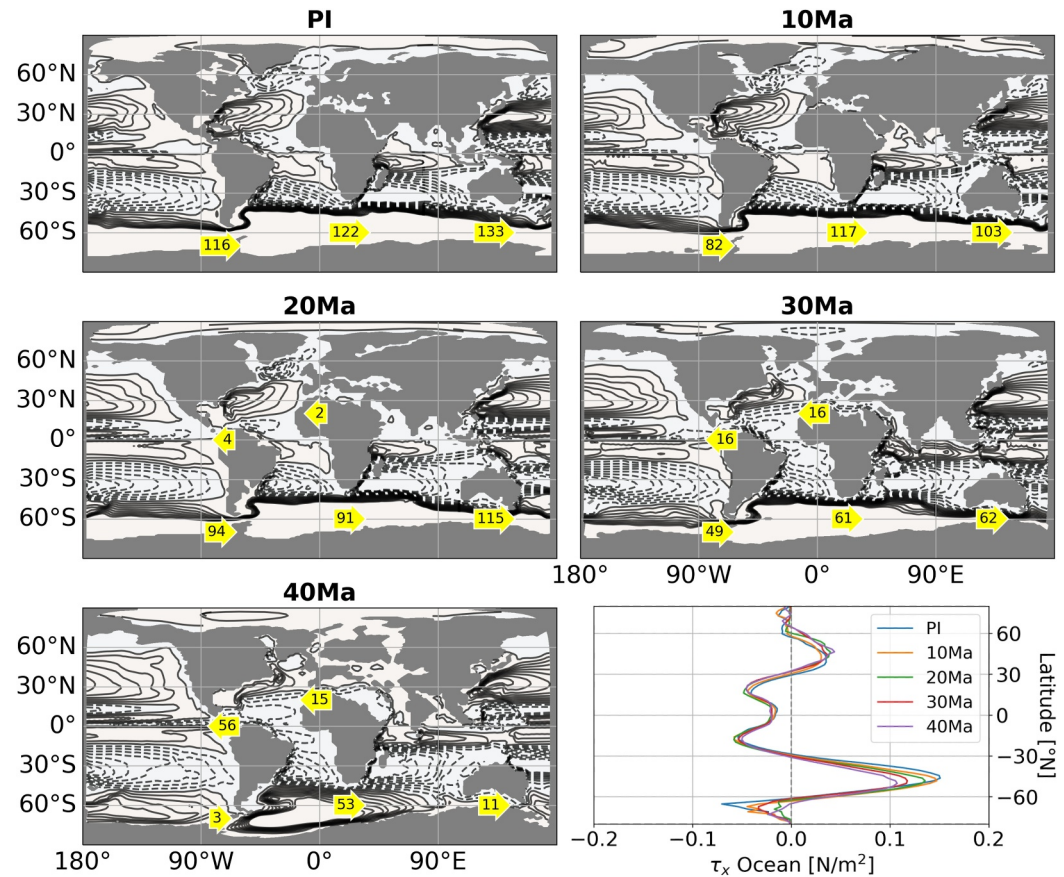
Figure 2. Barotropic Stream-function and eastward fluxes via Drake Passage, between Antarctica and Africa, via the Tasman Gateway and westward fluxes via Gibraltar and the CAS expressed in Sv. The bottom right panel shows the zonal wind-stress over the ocean averaged over the longitudes for PI (blue), 10 Ma (orange), 20 Ma (green), 30 Ma (red), and 40 Ma (purple).

changes emphasize the significant impact of bathymetry and topography on the ocean circulation. The ocean circulation response to pCO_2 changes is relatively weak under warm climatic conditions with the IPSL CM5A2 model (Zhang et al., 2020). In the PI, 10 and 20 Ma simulations, the lower branch of the AMOC flows southward and upwells between the ACC and the South Atlantic subtropical gyre, along the zero line contour of the BSF (Figures 1 and 2, Figure S7 in Supporting Information S1). The ACC volume transport (estimated between South Africa and Antarctica) increases progressively over the Cenozoic, rising from 61 Sv at 30 Ma to 122 Sv at PI. This intensification of the ACC occurs despite the Drake Passage being deeper at 30 Ma (4,750 m) than at 20 Ma (4,250 m), which contrasts with the findings of Sauermilch et al. (2021). However, their study examined much shallower Drake Passage depths (300, 600, and 1,000 m), resulting in much more pronounced transport changes than in the case of the deeper depths used here. In addition, the Drake Passage widens and becomes better aligned with the southern westerly wind maximum (~55–62°S; Figure 2 and Figure S3 in Supporting Information S1), contributing to the observed intensification. During the EOT, the global cooling has been suggested to enhance sea ice formation and brine rejection, which steepens isopycnals and further strengthens the ACC (Lefebvre et al., 2012). Our simulations also exhibit an expansion of the winter sea ice extent in the Southern Ocean (Figure S6 in Supporting Information S1), as well as a steepening of the isopycnals (Figure 1). At low latitudes, the CAS, Gibraltar Strait, and the Eastern Tethys Seaway remain open at 30 and 40 Ma, enabling a Circum-Equatorial Current (CEC) (Figure 2). Westward flows through the CAS reach 16 and 56 Sv, and 16 and 15 Sv through Gibraltar for 30 Ma and 40 Ma, respectively. At 20 Ma, the Eastern Tethys Seaway is closed, disrupting this CEC. However, a residual westward transport persists through the CAS (4 Sv) and Gibraltar (2 Sv).

Our simulations exhibit significant changes of the AMOC structure, along with a slowing down of the CEC and an intensification of the ACC across the Cenozoic. The evaluation of the ratio of ACC to AMOC volume transport (D. P. Marshall & Johnson, 2017) allow us to describe the evolution of the dynamical connections between the
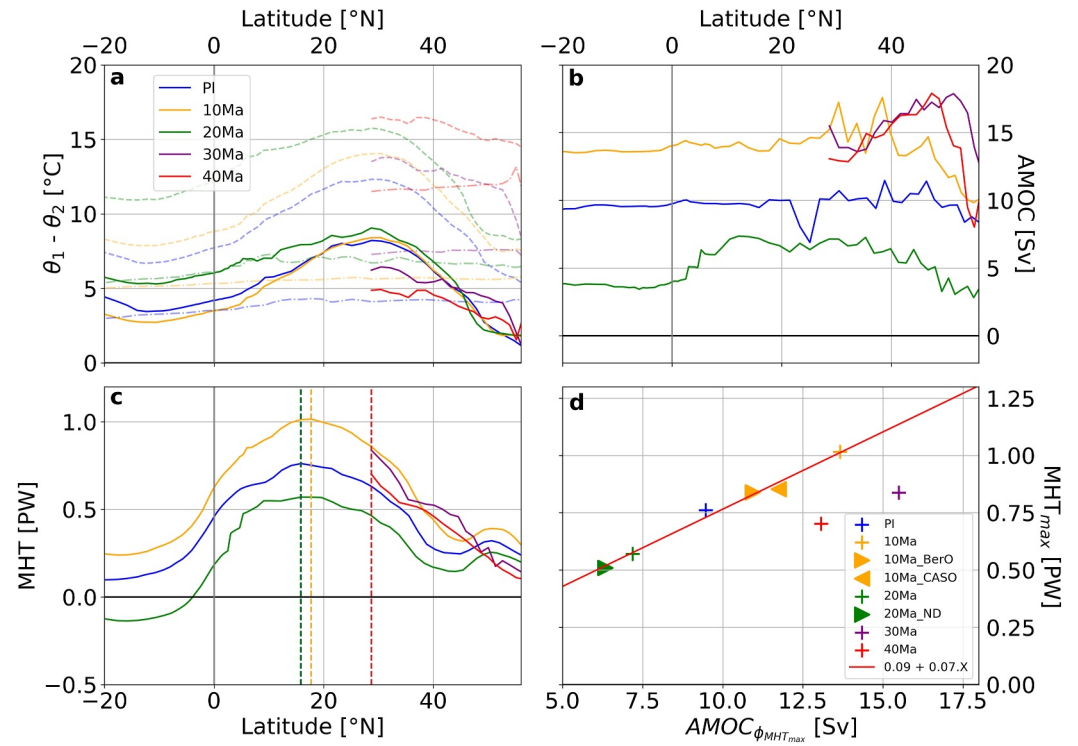
Figure 3. Averaged temperature differences between the upper limb (50–1,000 m) and the lower limb (1,000–2,500 m) in the Atlantic, the temperature of the upper limb is represented by the dashed lines and by the dash-doted lines for the lower limb (a), Atlantic Meridional Overturning Circulation (AMOC) (b), meridional heat transport (MHT) in the Atlantic (c). The variables are only represented north of the Gibraltar Strait for 30 and 40 Ma. MHT and AMOC at the latitude of the maximum MHT (d). The linear regression is calculated with the five simulations at the PI, 10, and 20 Ma (red line). The latitudes of the maximum MHT are represented on panel c with an overlap between PI and 20 Ma and between 30 and 40 Ma.

ACC and the AMOC during the Cenozoic (Table 1). The ratio is 11 in the PI simulation, between 8 and 9 in the 10 Ma experiments, between 10 and 11 in the 20 Ma experiments, all consistent with the present-day estimate of 8 ± 4 (D. P. Marshall & Johnson, 2017). In contrast, lower ratios of 3 are obtained for both the 30 Ma and 40 Ma simulations, when the CEC is active. These lower ratios are due to the AMOC becoming stronger and the ACC becoming weaker. The theoretical explanation for the 8 ± 4 ratio in the present-day ocean (D. P. Marshall & Johnson, 2017) relies on various assumptions (e.g., similar density profiles on the eastern boundary of the Atlantic from 35°S to 40°N, a weak stratification south of the ACC (D. P. Marshall & Johnson, 2017), which can be broken under different paleo configurations. For instance, the open equatorial seaways promoting the CEC at 30 and 40 Ma tend to upwell the pycnocline via an Ekman transport induced by the trade winds, and break down the hypothesis made of a quasi-constant density profile at the Atlantic eastern boundary. The linkage between the AMOC and the CEC likely depends on the depth of the pycnocline in low-latitude regions (Figure 1). However, establishing a robust scaling similar to the one done by D. P. Marshall and Johnson (2017) is challenging, as the CEC is not fully zonal but rather meanders in latitudes by tens of degrees, implying that its dynamics are also linked to wind-driven gyres.

Simulated changes in the AMOC structure are expected to impact the ocean heat transport, as in the present day climate, there is a strong correlation between AMOC intensity and MHT (Terhaar et al., 2025; Wang et al., 2023). Yet, it remains unknown if this correlation holds in previous climates. Following Wang et al. (2023), the MHT depends on the transport in the upper branch of the AMOC (V_1) and on the temperature difference between the upper $(\overline{\theta_1})$ and the lower branch of the AMOC $(\overline{\theta_2})$:

$$MHT \approx \rho \; C_p \; V_1 \; \left(\overline{\theta_1} - \overline{\theta_2}\right) \tag{2}$$

with ρ the seawater density, C_p its heat capacity.

In all simulations, the temperature differences increase from the equator to 30°N, before decreasing further north (Figure 3a). The AMOC remains relatively uniform meridionally in the PI, 10, and 20 Ma simulations (Figure 3b). The MHT increases between 20°S and 20°N, before decreasing at higher northern latitudes (Figure 3c). Our set of experiments shows very similar temperature differences at the latitude of the maximum MHT at PI, 10, and 20 Ma (Figure 3a), while the AMOC is 10, 14 and 10 Sv at PI, 10, and 20 Ma, respectively (Figure 3b). The MHT is 0.75, 1 and 0.55 PW at PI, 10 and 20 Ma, respectively (Figure 3c), resulting in a scaling of 0.07 PW/Sv for the six experiments at PI, 10 Ma and 20 Ma. This result is similar to the scaling of 0.05–0.08 PW/Sv found from observations and models for the modern climate (Wang et al., 2023). At 30 and 40 Ma, the AMOC at the latitude of maximum MHT is 16 and 13 Sv and the maximum MHT is 0.84 and 0.7 PW, respectively (Figure 3b–3d), while the predicted MHT from the scaling of Wang et al. (2023) would have been 1.2 and 1 PW. These large differences suggest that the sensitivity of the MHT to the AMOC intensity has changed across the Cenozoic. At 30 and 40 Ma, AMOC intensities are comparable to that at 10 Ma (14 Sv). However, the MHT is also influenced by the temperature contrast between the upper and the lower limb (6.2°C at 30 Ma and 4.9°C at 40 Ma, both lower than 6.9°C at 10 Ma). The reduced temperature anomaly at 30 and 40 Ma is likely associated with the position of the MHT maximum further north (~29°N) and a more homogeneous water column. In addition, substantial changes in wind-driven gyres further affect the MHT (Figure 2).

4. Conclusions and Discussion

The set of simulations presented in this study enhances our understanding of past ocean circulation by providing simulated climates across consistent paleogeographic configurations from 40 Ma to the PI period using a single model, thereby avoiding inter-model differences arising from varying parameterizations, resolutions and bathymetry. However, we acknowledge that comparing simulations with different paleogeographies, pCO$_2$, and ice-sheet configurations complicates the isolation of the individual impacts of these parameters on the climate. It would therefore be important to test the robustness of our results by conducting additional sensitivity experiments that vary only one parameter at a time.

The simulations of DeepMIP and MioMIP show substantial variability in ocean circulation for given time periods, with some models producing an AMOC, a PMOC and/or a SOMOC (Naik et al., 2025; Zhang et al., 2022), while all our simulations show deep water formation occurring only in the North Atlantic. These inter-model discrepancies are likely due to differences in spatial resolution, vertical mixing parameterizations, buoyancy forcing and paleogeographic reconstructions (Naik et al., 2025; Zhang et al., 2022). To improve our understanding of these dependencies, future MIP efforts should focus on assess quantities that encapsulating the dynamics at play in the ocean, such as the ratio between ACC and AMOC transports for simulations with closed equatorial seaways, as well as the relationship between AMOC strength and MHT, enabling more robust comparisons across experiments.

While the importance of the opening Southern Ocean gateways on the AMOC intensity has been widely acknowledged in the literature (Roquet et al., 2025), the role of the low-latitude gateways opening has seldom been examined. Our set of experiments shows that over the past 20 million years, NADW predominantly upwells in the Southern Ocean, when the Drake Passage is aligned with the southern westerly winds. This configuration coincides with a quasi-constant ratio between the ACC and AMOC transports, comparable to the present day ratio (D. P. Marshall & Johnson, 2017), suggesting that the dynamical connections between the ACC and the AMOC holds since the Miocene. In contrast, prior to 20 Ma, the ratio between the ACC and AMOC transports was much weaker certainly due to the low latitude upwelling of the NADW, supported by a circulation system we refer to as the CEC. Analogously to the ACC, the CEC likely facilitated NADW upwelling via Ekman divergence, this time induced by the trade winds. This results in a stronger-than-modern surface divergence on both sides of the Equator, replenished by mid-depth water masses.

Our study emphasizes that the three-dimensional structure of ocean circulation has undergone substantial changes throughout the Cenozoic. Initially characterized by a deep, single-hemispheric proto-AMOC cell and a vigorous SOMOC, the system evolved into an inter-hemispheric AMOC superimposed over a weaker SOMOC. This transition is crucial to consider when interpreting paleo-circulation proxy data. For example, the negative excursion of $\delta^{13}C$ observed in benthic foraminifera in the North Atlantic during the Oligocene has been attributed

to the southward export of NADW (or North Component Water, NCW), driven by the opening of the Drake Passage and the intensification of the ACC (Borrelli et al., 2014; Katz et al., 2011). However, our simulations suggest that during the Oligocene, NADW primarily upwelled at low latitudes, challenging the idea that wind-driven deep Southern Ocean upwelling was the dominant mechanism at that time. In addition, Abelson and Erez (2017) suggest that, 100–300 kyr before the EOT, the AMOC transitioned from a single-hemispheric to an inter-hemispheric circulation, as inferred from $\delta^{13}C$, $\delta^{18}O$, and Nd isotopes in the North and South Atlantic. Our simulations suggest that the AMOC was confined to the Northern Hemisphere prior to the Miocene, before the closure of the low-latitude straits. After the closure of the low-latitude connection between the Atlantic and the Indian oceans via the Tethys Sea, the long-term decline in radiogenic Nd in the Atlantic sector of the Southern Ocean during the late Oligocene and early Miocene has been attributed to enhanced NADW export (Scher & Martin, 2008) and is consistent with our findings.

Understanding the past controls of the AMOC can help predict its future stability, which is particularly important given ongoing debate about the risk of approaching an AMOC tipping point (van Westen et al., 2024).

Conflict of Interest

The authors declare no conflicts of interest relevant to this study.

Data Availability Statement

LMDZ, NEMO, and XIOS are released under the terms of the CeCILL license. OASIS-MCT is released under the terms of the Lesser GNU General Public License (LGPL). IPSL-CM5A2 source code is available at http://forge. ipsl.fr/igcmg/browser/CONFIG/publications/IPSLCM5A2_modipsl_rev6039_2023. The model outputs used in this study are accessible at Pineau (2025).

References

Abelson, M., & Erez, J. (2017). The onset of modern-like Atlantic meridional overturning circulation at the Eocene-Oligocene transition: Evidence, causes, and possible implications for global cooling. *Geochemistry, Geophysics, Geosystems*, *18*(6), 2177–2199. https://doi.org/10.1002/2017GC006826

Aminov, J., Dupont-Nivet, G., Ruiz, D., & Gailleton, B. (2023). Paleogeographic reconstructions using qgis: Introducing terra antiqua plugin and its application to 30 and 50 ma maps. *Earth-Science Reviews*, *240*, 104401. https://doi.org/10.1016/j.earscirev.2023.104401

Borrelli, C., Cramer, B. S., & Katz, M. E. (2014). Bipolar Atlantic deepwater circulation in the middle-late Eocene: Effects of Southern Ocean gateway openings. *Paleoceanography*, *29*(4), 308–327. https://doi.org/10.1002/2012PA002444

Boyle, P. R., Romans, B. W., Tucholke, B. E., Norris, R. D., Swift, S. A., & Sexton, P. F. (2017). Cenozoic North Atlantic deep circulation history recorded in contourite drifts, offshore Newfoundland, Canada. *Marine Geology*, *385*, 185–203. https://doi.org/10.1016/j.margeo.2016.12.014

Cessi, P. (2019). The global overturning circulation. *Annual Review of Marine Science*, *11*(1), 249–270. https://doi.org/10.1146/annurev-marine-010318-095241

Coxall, H. K., Huck, C. E., Huber, M., Lear, C. H., Legarda-Lisarri, A., O'Regan, M., et al. (2018). Export of nutrient rich Northern Component Water preceded early Oligocene Antarctic glaciation. *Nature Geoscience*, *11*(3), 190–196. https://doi.org/10.1038/s41561-018-0069-9

de Boer, A. M., Krishnan, S., Burls, N. J., Hutchinson, D. K., & Renoult, M. (2025). Evaluation of quasi-equilibrium criteria for coupled climate model simulations. *Geophysical Research Letters*, *52*(22), e2025GL117040. https://doi.org/10.1029/2025GL117040

Ferreira, D., Cessi, P., Coxall, H. K., De Boer, A., Dijkstra, H. A., Drijfhout, S. S., et al. (2018). Atlantic-Pacific Asymmetry in deep water Formation. *Annual Review of Earth and Planetary Sciences*, *46*(1), 327–352. https://doi.org/10.1146/annurev-earth-082517-010045

Fichefet, T., & Maqueda, M. A. M. (1997). Sensitivity of a global sea ice model to the treatment of ice thermodynamics and dynamics. *Journal of Geophysical Research*, *102*(C6), 12609–12646. https://doi.org/10.1029/97JC00480

Gnanadesikan, A. (1999). A simple predictive model for the structure of the Oceanic pycnocline. *Science*, *283*(5410), 2077–2079. https://doi.org/10.1126/science.283.5410.2077

Hohbein, M. W., Sexton, P. F., & Cartwright, J. A. (2012). Onset of North Atlantic Deep Water production coincident with inception of the Cenozoic global cooling trend. *Geology*, *40*(3), 255–258. https://doi.org/10.1130/G32461.1

Hotinski, R. M., & Toggweiler, J. R. (2003). Impact of a tethyan circumglobal passage on ocean heat transport and "equable" climates. *Paleoceanography*, *18*(1), 1007. https://doi.org/10.1029/2001PA000730

Hourdin, F., Foujols, M.-A., Codron, F., Guemas, V., Dufresne, J.-L., Bony, S., et al. (2013). Impact of the LMDZ atmospheric grid configuration on the climate and sensitivity of the IPSL-CM5A coupled model. *Climate Dynamics*, *40*(9–10), 2167–2192. https://doi.org/10.1007/s00382-012-1411-3

Hutchinson, D. K., Coxall, H. K., Lunt, D. J., Steinthorsdottir, M., de Boer, A. M., Baatsen, M., et al. (2021). The Eocene–Oligocene transition: A review of marine and terrestrial proxy data, models and model–data comparisons. *Climate of the Past*, *17*(1), 269–315. https://doi.org/10.5194/cp-17-269-2021

Hutchinson, D. K., de Boer, A. M., Coxall, H. K., Caballero, R., Nilsson, J., & Baatsen, M. (2018). Climate sensitivity and meridional overturning circulation in the late Eocene using GFDL CM2.1. *Climate of the Past*, *14*(6), 789–810. https://doi.org/10.5194/cp-14-789-2018

Jaramillo, C. A. (2018). *Evolution of the isthmus of Panama: Biological, paleoceanographic and paleoclimatological implications*. John Wiley and Sons.

Johnson, H. L., Cessi, P., Marshall, D. P., Schloesser, F., & Spall, M. A. (2019). Recent contributions of theory to our understanding of the Atlantic meridional overturning circulation. *Journal of Geophysical Research: Oceans*, *124*(8), 5376–5399. https://doi.org/10.1029/2019JC015330

Katz, M. E., Cramer, B. S., Toggweiler, J. R., Esmay, G., Liu, C., Miller, K. G., et al. (2011). Impact of Antarctic circumpolar Current development on late Paleogene Ocean structure. *Science*, *332*(6033), 1076–1079. https://doi.org/10.1126/science.1202122

Kirillova, V., Osborne, A. H., Störling, T., & Frank, M. (2019). Miocene restriction of the Pacific-North Atlantic throughflow strengthened Atlantic overturning circulation. *Nature Communications*, *10*(1), 4025. https://doi.org/10.1038/s41467-019-12034-7

Klocker, A., Munday, D., Gayen, B., Roquet, F., & LaCasce, J. H. (2023). Deep-Reaching Global Ocean overturning circulation generated by surface buoyancy forcing. *Tellus A: Dynamic Meteorology and Oceanography*, *75*(1), 392–409. https://doi.org/10.16993/tellusa.3231

Krinner, G., Viovy, N., De Noblet-Ducoudré, N., Ogée, J., Polcher, J., Friedlingstein, P., et al. (2005). A dynamic global vegetation model for studies of the coupled atmosphere-biosphere system: Dvgm for coupled climate studies. *Global Biogeochemical Cycles*, *19*(1), GB1015. https://doi.org/10.1029/2003GB002199

Labails, C., Olivet, J.-L., Aslanian, D., & Roest, W. R. (2010). An alternative early opening scenario for the Central Atlantic Ocean. *Earth and Planetary Science Letters*, *297*(3), 355–368. https://doi.org/10.1016/j.epsl.2010.06.024

Lefebvre, V., Donnadieu, Y., Sepulchre, P., Swingedouw, D., & Zhang, Z.-S. (2012). Deciphering the role of southern gateways and carbon dioxide on the onset of the Antarctic Circumpolar Current. *Paleoceanography*, *27*(4), PA4201. https://doi.org/10.1029/2012PA002345

Madec, G., Bourdallé-Badie, R., Bouttier, P.-A., Bricaud, C., Bruciaferri, D., Calvert, D., et al. (2016). NEMO ocean engine.

Marshall, D. P., & Johnson, H. L. (2017). Relative strength of the antarctic circumpolar current and atlantic meridional overturning circulation. *Tellus A: Dynamic Meteorology and Oceanography*, *69*(1), 1338884. https://doi.org/10.1080/16000870.2017.1338884

Marshall, J., & Speer, K. (2012). Closure of the meridional overturning circulation through Southern Ocean upwelling. *Nature Geoscience*, *5*(3), 171–180. https://doi.org/10.1038/ngeo1391

Meyssignac, B., Boyer, T., Zhao, Z., Hakuba, M. Z., Landerer, F. W., Stammer, D., et al. (2019). Measuring global ocean heat content to estimate the earth energy imbalance. *Frontiers in Marine Science*, *6*, 6–2019. https://doi.org/10.3389/fmars.2019.00432

Naik, T. J., de Boer, A. M., Coxall, H. K., Burls, N. J., Bradshaw, C. D., Donnadieu, Y., et al. (2025). Ocean meridional overturning circulation during the early and middle miocene. *Paleoceanography and Paleoclimatology*, *40*(4), e2024PA005055. https://doi.org/10.1029/2024PA005055

Nayak, M. S., Bonan, D. B., Newsom, E. R., & Thompson, A. F. (2024). Controls on the strength and structure of the Atlantic meridional overturning circulation in climate models. *Geophysical Research Letters*, *51*(11), e2024GL109055. https://doi.org/10.1029/2024GL109055

Nikurashin, M., & Vallis, G. (2012). A theory of the interhemispheric meridional overturning circulation and associated stratification. *Journal of Physical Oceanography*, *42*(10), 1652–1667. https://doi.org/10.1175/JPO-D-11-0189.1

Pineau, E. (2025). Amoc evolution across the Cenozoic through a shift of the isopycnal upwelling from the equator to the Southern Ocean [Dataset]. *Zenodo*. https://doi.org/10.5281/zenodo.16917981

Poblete, F., Dupont-Nivet, G., Licht, A., van Hinsbergen, D. J. J., Roperch, P., Mihalynuk, M. G., et al. (2021). Towards interactive global paleogeographic maps, new reconstructions at 60, 40 and 20 Ma. *Earth-Science Reviews*, *214*, 103508. https://doi.org/10.1016/j.earscirev.2021.103508

Roquet, F., Bell, M. J., de Boer, A. M., Ferreira, D., Jones, C. S., LaCasce, J. H., et al. (2025). Controls of the global overturning circulation of the ocean. *npj Climate and Atmospheric Science*, (Vol. 8(Iss. 1)), 304. (Publisher: Nature Publishing Group). https://doi.org/10.1038/s41612-025-01185-8

Sauermilch, I., Whittaker, J. M., Klocker, A., Munday, D. R., Hochmuth, K., Bijl, P. K., & LaCasce, J. H. (2021). Gateway-driven weakening of ocean gyres leads to Southern Ocean cooling. *Nature Communications*, *12*(1), 6465. https://doi.org/10.1038/s41467-021-26658-1

Scher, H. D., & Martin, E. E. (2008). Oligocene deep water export from the North Atlantic and the development of the Antarctic Circumpolar Current examined with neodymium isotopes. *Paleoceanography*, *23*(1), PA1205. https://doi.org/10.1029/2006PA001400

Sepulchre, P., Caubel, A., Ladant, J.-B., Bopp, L., Boucher, O., Braconnot, P., et al. (2020). IPSL-CM5A2 – An Earth system model designed for multi-millennial climate simulations. *Geoscientific Model Development*, *13*(7), 3011–3053. https://doi.org/10.5194/gmd-13-3011-2020

Shakespeare, C. J., & Hogg, A. M. (2012). An analytical model of the response of the meridional overturning circulation to changes in wind and buoyancy forcing. *Journal of Physical Oceanography*, *42*(8), 1270–1287. https://doi.org/10.1175/JPO-D-11-0198.1

Straume, E. O., Gaina, C., Medvedev, S., & Nisancioglu, K. H. (2020). Global Cenozoic Paleobathymetry with a focus on the Northern Hemisphere Oceanic Gateways. *Gondwana Research*, *86*, 126–143. https://doi.org/10.1016/j.gr.2020.05.011

Straume, E. O., Nummelin, A., Gaina, C., & Nisancioglu, K. H. (2022). Climate transition at the Eocene–Oligocene influenced by bathymetric changes to the Atlantic–Arctic oceanic gateways. *Proceedings of the National Academy of Sciences*, *119*(17), e2115346119. https://doi.org/10.1073/pnas.2115346119

Talley, L. (2013). Closure of the global overturning circulation through the Indian, Pacific, and Southern Oceans: Schematics and transports. *Oceanography*, *26*(1), 80–97. https://doi.org/10.5670/oceanog.2013.07

Terhaar, J., Vogt, L., & Foukal, N. P. (2025). Atlantic overturning inferred from air-sea heat fluxes indicates no decline since the 1960s. *Nature Communications*, *16*(1), 222. https://doi.org/10.1038/s41467-024-55297-5

Thomas, D. J., Korty, R., Huber, M., Schubert, J. A., & Haines, B. (2014). Nd isotopic structure of the Pacific Ocean 70–30 Ma and numerical evidence for vigorous ocean circulation and ocean heat transport in a greenhouse world. *Paleoceanography*, *29*(5), 454–469. https://doi.org/10.1002/2013PA002535

Vahlenkamp, M., Niezgodzki, I., De Vleeschouwer, D., Lohmann, G., Bickert, T., & Pälike, H. (2018). Ocean and climate response to North Atlantic seaway changes at the onset of long-term Eocene cooling. *Earth and Planetary Science Letters*, *498*, 185–195. https://doi.org/10.1016/j.epsl.2018.06.031

van Westen, R. M., Kliphuis, M., & Dijkstra, H. A. (2024). Physics-based early warning signal shows that amoc is on tipping course. *Science Advances*, *10*(6), eadk1189. https://doi.org/10.1126/sciadv.adk1189

von der Heydt, A., & Dijkstra, H. A. (2008). The effect of gateways on ocean circulation patterns in the cenozoic. *Global and Planetary Change*, *62*(1), 132–146. https://doi.org/10.1016/j.gloplacha.2007.11.006

Wang, F., Xu, X., Zhang, F., & Ma, L. (2023). Structure of the atlantic meridional overturning circulation in three generations of climate models. *Earth and Space Science*, *10*(7), e2023EA002887. https://doi.org/10.1029/2023EA002887

Zhang, Y., Boer, A. M., Lunt, D. J., Hutchinson, D. K., Ross, P., Flierdt, T., et al. (2022). Early Eocene Ocean meridional overturning circulation: The roles of atmospheric forcing and Strait geometry. *Paleoceanography and Paleoclimatology*, *37*(3), e2021PA004329. https://doi.org/10.1029/2021PA004329

Zhang, Y., Huck, T., Lique, C., Donnadieu, Y., Ladant, J.-B., Rabineau, M., & Aslanian, D. (2020). Early Eocene vigorous ocean overturning and its contribution to a warm Southern Ocean. *Climate of the Past*, *16*(4), 1263–1283. https://doi.org/10.5194/cp-16-1263-2020

References From the Supporting Information

Bintanja, R., van der Wiel, K., van der Linden, E. C., Reusen, J., Bogerd, L., Krikken, F., & Selten, F. M. (2020). Strong future increases in arctic precipitation variability linked to poleward moisture transport. *Science Advances*, *6*(7), eaax6869. https://doi.org/10.1126/sciadv.aax6869

Brierley, C. M., & Fedorov, A. V. (2016). Comparing the impacts of Miocene–Pliocene changes in inter-ocean gateways on climate: Central american seaway, bering strait, and Indonesia. *Earth and Planetary Science Letters*, *444*, 116–130. https://doi.org/10.1016/j.epsl.2016.03.010

Burls, N. J., Bradshaw, C. D., De Boer, A. M., Herold, N., Huber, M., Pound, M., et al. (2021). Simulating miocene warmth: Insights from an opportunistic multi-model ensemble (miomip1). *Paleoceanography and Paleoclimatology*, *36*(5), e2020PA004054. https://doi.org/10.1029/2020PA004054

Caballero, R., & Huber, M. (2013). State-dependent climate sensitivity in past warm climates and its implications for future climate projections. *Proceedings of the National Academy of Sciences*, *110*(35), 14162–14167. https://doi.org/10.1073/pnas.1303365110

Hall, J. R., Allison, M. S., Papadopoulos, M. T., Barfod, D. N., & Jones, S. M. (2023). Timing and consequences of bering strait opening: New insights from 40ar/39ar dating of the barmur group (tjörnes beds), northern Iceland. *Paleoceanography and Paleoclimatology*, *38*(4), e2022PA004539. https://doi.org/10.1029/2022PA004539

Hu, A., Meehl, G. A., Han, W., Otto-Bliesner, B., Abe-Ouchi, A., & Rosenbloom, N. (2015). Effects of the bering strait closure on amoc and global climate under different background climates. *Progress in Oceanography*, *132*, 174–196. (Oceanography of the Arctic and North Atlantic Basins). https://doi.org/10.1016/j.pocean.2014.02.004

Inglis, G. N., Bragg, F., Burls, N. J., Cramwinckel, M. J., Evans, D., Foster, G. L., et al. (2020). Global mean surface temperature and climate sensitivity of the early eocene climatic optimum (eeco), Paleocene–Eocene thermal maximum (petm), and latest paleocene. *Climate of the Past*, *16*(5), 1953–1968. https://doi.org/10.5194/cp-16-1953-2020

Khon, V. C., Hoogakker, B. A. A., Schneider, B., Segschneider, J., & Park, W. (2023). Effect of an open central american seaway on ocean circulation and the oxygen minimum zone in the tropical pacific from model simulations. *Geophysical Research Letters*, *50*(20), e2023GL103728. https://doi.org/10.1029/2023GL103728

Lagabrielle, Y., Goddéris, Y., Donnadieu, Y., Malavieille, J., & Suarez, M. (2009). The tectonic history of Drake Passage and its possible impacts on global climate. *Earth and Planetary Science Letters*, *279*(3), 197–211. https://doi.org/10.1016/j.epsl.2008.12.037

Lunt, D. J., Bragg, F., Chan, W.-L., Hutchinson, D. K., Ladant, J.-B., Morozova, P., et al. (2021). Deepmip: Model intercomparison of early eocene climatic optimum (eeco) large-scale climate features and comparison with proxy data. *Climate of the Past*, *17*(1), 203–227. https://doi.org/10.5194/cp-17-203-2021

Montes, C., Cardona, A., Jaramillo, C., Pardo, A., Silva, J. C., Valencia, V., et al. (2015). Middle Miocene closure of the Central American Seaway. *Science*, *348*(6231), 226–229. https://doi.org/10.1126/science.aaa2815

O'Brien, C. L., Huber, M., Thomas, E., Pagani, M., Super, J. R., Elder, L. E., & Hull, P. M. (2020). The enigma of oligocene climate and global surface temperature evolution. *Proceedings of the National Academy of Sciences*, *117*(41), 25302–25309. https://doi.org/10.1073/pnas.2003914117

Pérez-Asensio, J. N., Aguirre, J., Schmiedl, G., & Civis, J. (2012). Impact of restriction of the atlantic-mediterranean gateway on the mediterranean outflow water and eastern atlantic circulation during the messinian. *Paleoceanography*, *27*(3), PA3222. https://doi.org/10.1029/2012PA002309

Pillot, Q., Donnadieu, Y., Sarr, A.-C., Ladant, J.-B., & Suchéras-Marx, B. (2022). Evolution of ocean circulation in the North Atlantic Ocean during the Miocene: Impact of the Greenland ice sheet and the eastern Tethys seaway. *Paleoceanography and Paleoclimatology*, *37*(8), e2022PA004415. https://doi.org/10.1029/2022PA004415

Valcke, S. (2013). The OASIS3 coupler: A European climate modelling community software. *Geoscientific Model Development*, *6*(2), 373–388. https://doi.org/10.5194/gmd-6-373-2013